

3 Libo Wang¹, Peter Toose¹, Ross Brown², and Chris Derksen¹

6 ² Climate Processes Section, Climate Research Division, Environment and Climate Change
7 Canada@Ouranos, Montreal, Québec, Canada

9

This study presents an algorithm for detecting winter melt events in seasonal snow cover based on temporal variations in the brightness temperature difference between 19 and 37 GHz from satellite passive microwave measurements. An advantage of the passive microwave approach is that it is based on the physical presence of liquid water in the snowpack, which may not be the case with melt events inferred from surface air temperature data. The algorithm is validated using in situ observations from weather stations, snowpit surveys, and a surface-based passive microwave radiometer. The results of running the algorithm over the pan-Arctic region (north of 50° N) for the 1988-2013 period show that winter melt days are relatively rare averaging less than 7 melt days per winter over most areas, with higher numbers of melt days (around two weeks per winter) occurring in more temperate regions of the Arctic (e.g. central Quebec and Labrador, southern Alaska, and Scandinavia). The observed spatial pattern was similar to winter melt events inferred with surface air temperatures from ERA-interim and MERRA reanalysis



23 datasets. There was little evidence of trends in winter melt frequency except decreases over
24 northern Europe attributed to a shortening of the duration of the winter period. The frequency of
25 winter melt events is shown to be strongly correlated to the duration of winter period. This must
26 be taken into account when analyzing trends to avoid generating false increasing trends from
27 shifts in the timing of the snow cover season.

28

29 **1. Introduction**

30 Snow cover is important in Arctic climate and ecological systems and has decreased in areal
31 extent and duration especially during the spring period in response to rapid Arctic warming in
32 recent decades [Brown and Robinson, 2011; Derksen and Brown, 2012; Callaghan et al. 2012].
33 The conventional wisdom is that Arctic warming will result in an increase in the frequency and
34 duration of winter melt events which may also include rain-on-snow (ROS) events. These winter
35 melt/refreeze events modify the physical properties of snow (albedo, density, grain size, thermal
36 conductivity), generate winter runoff [Bulygina et al., 2010; Johansson et al., 2011] and can
37 result in potentially significant impacts on the surface energy budget, hydrology and soil thermal
38 regime [Boon et al., 2003; Hay and McCabe, 2010; Rennert et al., 2009]. The refreezing of melt
39 water can also create ice layers that adversely impact the ability of ungulate travel and foraging
40 [Hansen et al., 2011; Grenfell and Putkonen, 2008], and exert uncertainties in snow mass
41 retrieval from passive microwave satellite data [Derksen et al., 2014; Rees et al., 2010]. Winter
42 warming and melt events may also damage shrub species and tree roots, affecting plant
43 phenology and reproduction in the Arctic [Bokhorst et al., 2009; AMAP, 2011]. However, little
44 is known about the spatial and temporal variability of winter melt events at the pan-Arctic scale.



45

46 Winter melt events are rare extreme events over most of the Arctic and are sporadic in time and
47 space [Pedersen et al., 2015]. These events are linked to intrusion of warm air from southerly or
48 southwesterly flow, may be associated with rain and/or freezing rain, and typically last for
49 several days. Previous studies [Cohen et al. 2015; Rennert et al 2009] have shown that the
50 synoptic conditions associated with these events project strongly onto larger modes of
51 atmospheric circulation.

52

53 Microwave remote sensing measurements are very sensitive to the presence of liquid water in
54 snow. Dry snow is a mixture of air and ice. Because the permittivity of water is much higher than
55 those of air and ice at microwave frequencies, the introduction of even a small amount of liquid
56 water (0.5%) in snow can increase the permittivity of snow by over an order of magnitude
57 [Ulaby et al., 1986]. This increases absorption and reduces the penetration depth, which in turn
58 results in a large increase in brightness temperature (T_B) and decrease in radar backscatter.
59 Satellite active and passive microwave measurements have been widely used for snow melt
60 detection over various components of the Arctic cryosphere during the spring melt period
61 [Markus et al., 2009; Tedesco, 2007; Kim et al., 2011, Wang et al., 2011]. Only a few satellite
62 studies have focused on winter melt detection, and are mainly based on active microwave
63 satellite data [Bartsch et al., 2010; Wilson et al., 2012; Semmens et al., 2013] for specific regions
64 and limited time periods. Here we develop an algorithm to detect winter melt from satellite
65 passive microwave (PMW) data over pan-Arctic land areas north of 50° N for the period 1988-
66 2013.

67



68 Winter melt and ROS events can also be inferred from surface weather observations [Groisman
69 et al., 2003; McBean et al., 2005; Pedersen et al., 2015], reanalyses [Cohen et al. 2015; Rennert
70 et al., 2009], or reanalysis-driven snowpack models [Liston and Hiemstra, 2010]. In most of
71 these studies, winter melt events are assumed to occur when the daily air temperature exceeds a
72 certain threshold. For example, Groisman et al. [2003] defined a thaw day as a day with snow on
73 the ground when the daily mean air temperature is above -2°C . Inferring thaw events from
74 surface air temperatures in this way does not consider the energy balance of the snowpack. In
75 addition, reanalysis datasets can contain important biases and inhomogeneity over the Arctic [e.g.
76 Rapaic et al. 2015] that will impact the spatial and temporal frequency of the inferred winter
77 thaw events. The advantage of the passive microwave approach described above is that melt
78 events are directly linked to the appearance of liquid water in snow which drives changes in
79 snowpack properties relevant to Arctic ecosystems. The brightness temperature series is also
80 considered to be consistent over the 1988-2013 period as it is derived from near identical
81 spaceborne sensors.

82

83 Previous studies have linked field observations of ice layer formation from ROS events with
84 satellite measurements [Bartsch et al., 2010; Grenfell and Putkonen, 2008], but few studies have
85 showed links between satellite measurements and in situ observations of changes in snow
86 properties from melt/refreeze events [Nghiem et al., 2014]. The passive microwave satellite data
87 used to detect changes in snow properties due to ROS or melt/refreeze events are in coarse
88 resolutions (10-25 km) with twice daily overpasses at the high latitudes. Thus melt events of
89 short duration or limited spatial distribution may not be detectable. The objectives of this study
90 are to (1) develop an algorithm for winter melt detection from PMW data, and (2) to characterize



91 winter melt events detectable by PMW at the satellite scale using surface-based PMW
 92 radiometer measurements and snowpit surveys collected during field campaigns. These results
 93 are compared to winter melt detection results inferred from near surface air temperature fields
 94 from two commonly used reanalysis datasets. Trends in PMW-derived winter melt frequency
 95 over the period 1988-2013 are presented along with a demonstration of the impact on trend
 96 results of using a fixed winter period for defining the snow season.

97

98 **2. Data and Methods**

99

100 **2.1. Satellite passive microwave data**

101

102 This study uses T_B data from the Special Sensor Microwave/Imager (SSM/I, 1987–2008), and
 103 the Special Sensor Microwave Imager/Sounder (SSMIS, 2009 to present) re-projected to 25 km
 104 EASE-Grid available from the National Snow and Ice Data Center in Boulder, Colorado
 105 [Armstrong et al., 1994]. These sensors provide a continuous time series of T_B since 1987 (Table
 106 1). We do not perform sensor cross calibration given that only small differences were found
 107 between sensors [Abdalati et al., 1995; Stroeve et al., 1998; Cavalieri et al., 2012]. Since our
 108 melt detection algorithm (described below) only uses the relative change in the temporal
 109 variations in T_B , slight offsets in absolute T_B between sensors should not affect algorithm
 110 performance. The gaps in the data are filled by linear interpolation from adjacent days. Vertically
 111 polarized T_B from afternoon overpasses are utilized to increase the likelihood of observing melt
 112 events, rather than morning overpasses. Due to large temporal gaps in the early SSM/I record
 113 (pre-1987), the time series used begin in the fall of 1988 and extend to 2014 (Table 1). Although



horizontal polarized measurements are more sensitive to ice lenses within the snowpack [Derksen et al., 2009; Rees et al., 2010], there is not much difference between the two polarizations for melt detection and we use vertically polarized measurements to be consistent with Wang et al. [2013].

2.2. Winter melt detection method for PMW

As the purpose of this study is to detect winter melt events, the winter period duration (WPD) is defined as occurring between the main snow onset date (MSOD) in the fall (beginning of continuous dry snow cover on the ground) and the main melt onset date (MMOD) in the spring (beginning of frequent melt/freeze diurnal cycles). Figure 1 illustrates the steps involved in detecting melt events for the WPD, based on the temporal variations in the difference of the brightness temperature (T_{BD}) between 19 and 37 GHz and a 37GHz T_B threshold. For dry snow conditions, as snow accumulates T_{BD} increases due to the larger scattering effect of the microwave signal by snow grains at 37 GHz versus 19 GHz [Chang et al., 1987]. Upon the appearance of liquid water in snow, T_B increases at both frequencies and results in a drop in T_{BD} , to similar magnitudes seen in snow free conditions, but will quickly revert back to dry snow T_{BD} levels once the snow re-freezes allowing for the detection of melt/re-freeze events (Figure 2).

The purpose of determining MSOD is to capture the earliest start date of the continuous dry snowpack. The MSOD is determined as the first date when (1) $T_{BD} \geq T_{sn}$ (a threshold = mean July $T_{BD} + 3.5$ K) for 7 out of 10 days and (2) $T_{B37v} < 253$ K for 10 out of 11 days (Figure 1). The thresholds and conditions were optimized by comparing the PMW determined MSOD to



137 daily snow depth observations from the Global Surface Summary of the Day dataset archived at
138 the National Climate Data Center (<http://www.ncdc.noaa.gov>). The T_B criterion in (2) is applied
139 to exclude periods with T_{BD} fluctuations related to early season freeze/thaw cycles because of its
140 sensitivity to the presence of liquid water in the snow (see below for its derivation).

141

142 MMOD is determined following Wang et al. [2013]. Their algorithm was based on temporal
143 variations in T_{BD} relative to the previous 3-day average T_{BD} (referred as M hereafter). Melt
144 onset was detected if the difference in M and daily T_{BD} was greater than a threshold ($TH_{old} =$
145 $0.35 \cdot M$) for four or more consecutive days. Based on trial and error, the MMOD detection
146 algorithm in Wang et al [2013] is modified here to detect mid-winter melt events that are
147 typically of shorter duration. Firstly, the threshold is modified slightly from $TH_{old} = 0.35 \cdot M$ to
148 $TH_{new} = 0.4 \cdot M$ since the goal is to detect melt events with one or more days of duration (instead
149 of four days as in the previous study, thus a more strict threshold here), and secondly, a T_{B37v}
150 threshold condition is added following Semmens et al. [2013] to mitigate false detection due to
151 T_{BD} changes not related to melt (e.g. noise). The resulting expression for winter melt event
152 conditions is $(M - T_{BD}) > TH_{new}$ and $T_{B37v} \geq 253$ K for one day (Figure 1, referred as the winter
153 T_{BD} algorithm hereafter). The $T_{B37v} \geq 253$ K condition was obtained by evaluating a range of
154 T_{B37v} values from 250-255 K, at 1 K increments to identify the threshold most sensitive to the
155 presence/absence of liquid water in snow. This was inferred from histograms of daily maximum
156 (T_{max}), mean (T_m), and minimum (T_{min}) air temperatures for days detected as melting at all
157 available stations during 2000-2007 (see locations in Figure 5b, ~5100 observations in total).
158 The results show that for $T_{B37v} = 253$ K, T_{max} is $\geq 0^\circ$ C for nearly 96% of cases, T_{min} is $< 0^\circ$
159 C for 94%, and T_m is $\geq 0^\circ$ C for 80%. This suggests that the PMW-detected winter melt events



160 are consistent with diurnal positive air temperature events, while most of the events (80%)
 161 probably last multiple hours thus corresponding to days with $T_m \geq 0^\circ \text{C}$. If a melt event is
 162 detected within 10 days from the MMOD, then it is not considered a mid-winter melt event, but
 163 rather a preliminary melt event to the MMOD and is excluded from the analysis.
 164
 165 An example of the performance of the winter T_B D algorithm is shown in Figure 2 for a case at
 166 Pudasjarvi, Finland (65.4°N , 26.97°E) during the 2013- 2014 winter. At Pudasjarvi station, the
 167 snow depth first became greater than 0 cm on day of year (DOY) 291 of 2013. The snow depth
 168 was mostly less than 10 cm for days 291 to 332, with two periods of no snow on the ground
 169 while T_{max} fluctuated around 0°C . The PMW detected MSOD was on DOY332, corresponding
 170 within 1 week of the date of continuous snow cover above 10 cm observed at the station (Figure
 171 2b). MMOD was detected on DOY64 of 2014, however, there was still snow on the ground until
 172 DOY108, typical of high latitude snow cover where melt onset is followed by the spring thaw,
 173 which is a sustained period with high diurnal air temperature variation where the snowpack is
 174 melting during the day and refreezing at night. At the end of this melt-refreeze period, the
 175 snowpack may be actively melting both day and night until snow disappearance which can take
 176 several weeks [Semmens et al., 2013]. During winter 2013-2014, 20 melt days in total were
 177 detected at Pudasjarvi, all corresponding to days with $T_{\text{max}} \geq 0^\circ \text{C}$. However, not all days with
 178 $T_{\text{max}} \geq 0^\circ \text{C}$ are detected by PMW as melting, for example DOY351-352, for reasons which
 179 will be explained further in the validation section.
 180
 181 The winter T_B D algorithm is applied to time series of T_B for each winter period over the period
 182 1988-2013. The WPD varies at each pixel and is determined by MSOD and MMOD as described



above. This approach is referred to as “PMW-varying” in the following analysis. Since we focus on melt events during the winter period, the T_B D algorithm is only applied to pixels with MSOD detected before the end of December and with MMOD later than March 1st, i.e. with WPD > 60 days. The PMW-varying approach is internally consistent in that it takes account of annual variations in winter temperature and snow cover. This is not the case for analysis using a fixed “winter” window where spurious trends can be created from changing seasonality (i.e. earlier snow melt). To highlight this, a fixed window approach is also applied (“PMW-fixed”) where the T_B D algorithm is applied to time series of T_B from November to April. The results presented in the following sections are from the PMW-varying method unless explicitly indicated otherwise. Since the microwave response of melt on permanent snow and ice is different from seasonal terrestrial snow cover, we mask out the Greenland Ice sheet and glaciers in our analyses.

2.3. Winter melt detection for reanalysis datasets

Winter melt event information from the $0.75^\circ \times 0.75^\circ$ degree latitude/longitude ERA-interim (ERA-I) [Dee et al., 2011] and the $1/2^\circ$ latitude by $2/3^\circ$ longitude MERRA [Rienecker et al 2011] reanalyses were used to evaluate the melt event climatology generated by the PMW method. Melt events in the reanalyses are inferred from 6-hourly air temperatures over the same period as the satellite data. For the comparison, a winter thaw event is defined as a period of above-freezing daily mean air temperature occurring during the period dominated by below-freezing air temperatures (defined by 0° C crossing dates obtained with a centered 30-day moving average of daily mean air temperature). This is analogous to the “PMW-varying” method described above. An additional condition is imposed of at least 10 cm snow depth for ERA-I or 4 mm SWE for



206 MERRA on the ground to obtain results comparable to the PMW method of detection over snow
 207 covered ground. The mean daily air temperature is the average of the 00, 06, 12 and 18 UTC
 208 values. Snow depths for ERA-I are taken from the daily snow depth reconstruction described in
 209 Brown and Derksen [2013] to avoid various inconsistencies with the snow depths in the
 210 reanalysis.

211

212 **2.4. In situ field observations and methods**

213

214 The satellite-based winter melt detection algorithm is validated with surface-based PMW
 215 radiometer measurements along with near surface air/snow temperature observations recorded on
 216 April 12th-13th, 2010 during a field campaign near Churchill, Manitoba, Canada [Derksen et al.,
 217 2012]. A modified version of the winter T_B D algorithm is applied to the surface-based
 218 radiometer measurements due to the continuous nature of the data. We simply used the average
 219 T_B values from the stable pre-melt period as our reference frozen T_B D value instead of previous
 220 3-day average.

221

222 Furthermore, we try to characterize winter melt events detectable by the winter T_B D algorithm
 223 using snowpit surveys recorded during multiple PMW snow measurement campaigns conducted
 224 between 2005 and 2010 in both the boreal forest and tundra environments of Canada (Table2).
 225 The number of satellite detected melt events for the specific EASE-Grid pixels surrounding the
 226 snow pit locations are compared to the number of melt forms/ice formations identified within the
 227 snowpack. A melt feature identified lower (closer to the ground) is consider an early winter event,
 228 while those melt features identified closer to the surface of the snow are considered more recent



229 events. An example of the coincident satellite, air temperature and snow pit information for a
 230 survey site near Thompson, Manitoba is shown in Figure 3. Hourly air temperatures from
 231 weather stations in the vicinity of the snow pits (within 70 km), are examined to identify if and
 232 when a melt event occurred in the region, how long the melt event lasted, what the average
 233 temperature was for the duration of the event and what the minimum, maximum and average 36
 234 hour air temperatures were preceding the melt event. Results of the field evaluation are presented
 235 in Section 3.1

236

237 **3. Results**

238

239 **3.1. Field evaluation of melt algorithm**

240

241 Figure 4 illustrates the time series of the surface-based radiometer T_B and temperature
 242 measurements recorded during the April 12th-13th Churchill melt event. The area in green
 243 highlights the period for which the modified T_B D algorithm identified the melt event. As the near
 244 surface air temperatures approached 0° C, T_B increased rapidly at both the 19 and 37 GHz. The
 245 detected melt onset occurred ~ 40 minutes after the 11 cm and 7 cm air temperatures crossed the
 246 0° C threshold and 25 minutes before the 2 m air temperature exceeded 0° C, likely due to
 247 radiant heating from the sun to the snow surface and the boundary layer air temperature probe.
 248 The -1 cm snow temperature didn't reach 0° C until three hours after the detected melt onset. The
 249 influence of radiant heating becomes obvious during the late afternoon/early evening, upon
 250 sunset (~1900 hr local) the snowpack and boundary layer air temperatures all drop below 0° C,
 251 closely followed by a gradual drop in the T_B signal even while the 2 m air temperatures are still



252 positive. Compared to the rapid increase in T_B during the melt onset, the more gradual decrease
253 in T_B is likely due to the mixed effects of uneven re-freezing of the snow surface and delayed
254 freezing of sub-surface liquid water.

255

256 The validation results using snowpit data are summarized in Table 2. The performance of the
257 winter T_B D algorithm is highlighted in green for a successful melt detection and in red for a
258 failed detection. The results suggest that a successful detection is likely when the melt duration
259 last for multiple hours (>6 hours) or multiple days, and/or the melt event has been preceded by
260 warm air temperatures that have warmed the snowpack to near melting conditions (previous
261 day's $T_{max} > -3^\circ \text{C}$). In these situations, it is common for melt features to form within the
262 snowpack. The algorithm does not reliably identify short duration melt events or events that
263 occur immediately after extremely cold air/snowpack temperatures (previous 36 hour minimum
264 air temperature $< -13^\circ \text{C}$). In these instances, the snowpack likely has enough thermal inertia to
265 remain within a frozen state for the whole duration of the melt event, or very quickly return to a
266 frozen state and thus liquid water is not detectable with satellite T_B .

267

268 The winter T_B D algorithm is also not well suited to detect ROS events and the subsequent
269 development of ice layers within the snowpack. The Daring Lake [Rees et al., 2010] and
270 LaGrande IV melt events presented in Table 2 were coincident with ROS, but were both quickly
271 followed by cold air temperatures leading to the re-freezing of the liquid water and were thus not
272 detected. The winter T_B D algorithm is very sensitive to liquid water within the snow, but does
273 not necessarily capture all events that can create melt features within the snowpack, largely due
274 to the timing of the satellite overpass (~1800 h local) and the coarse resolution (25 km).



275

276 3.2. The spatial distribution of winter melt events

277

278 Figure 5 shows the PMW-derived MSOD, MMOD, and WPD during the 1988-2013 period. On
 279 average, continuous snow cover starts in the Canadian Arctic islands and high elevation regions
 280 of the Arctic in September and progresses to the open tundra in October (Figure 5a). By
 281 November, most of the areas north of 50° N are covered by snow except for some temperate
 282 maritime and lower latitude regions where continuous snow cover sets in December. The spring
 283 main melt onset starts at lower latitudes in March, progresses to the boreal forests and tundra in
 284 April/May, and reaches the high Arctic in June (Figure 5b), giving rise to spatial variability in
 285 the duration of the winter period from one to seven months on average (Figure 5c). A pixel-wise
 286 definition of winter period for winter melt detection is required to account for this spatial
 287 variability as well as the temporal variability from year-to-year fluctuations in snow cover.

288

289 During the 26 winters, melt occurred at least once everywhere north of 50° N using the PMW-
 290 varying window method (Figure 6a). However, the average number of melt days is less than one
 291 week per winter for most areas, with more melt days (around two weeks per winter) occurring in
 292 areas with a relatively long snow season and more temperate winter climates (e.g. central Quebec
 293 and Labrador, southern Alaska, and Scandinavia). The spatial distribution patterns of NMD from
 294 ERA-I (Figure 6c) and MERRA (Figure 6d) generally agree with that from PMW. However,
 295 ERA-I detects about one week more melt days on average in most areas, while MERRA detects
 296 less melt days in Quebec and central Canada relative to PMW. Both ERA-I and MERRA detect
 297 more melt days in southern Alaska and western North America (NA). These are relatively deep



298 snowpack regions where melt may not occur in short periods of freezing air temperatures due to
 299 the thermal inertia of the snowpack. Compared to the PMW-varying window method (Figure 6a),
 300 there are many more melt days detected using the PMW-fixed window method (Figure 6b),
 301 especially in the relatively temperate climate regions (e.g. northern Europe and lower latitudes of
 302 NA and Russia) where the WPD is relatively short and thus limits the possible number of melt
 303 days to be detected.

304

305 Figure 7 shows the monthly mean NMD from October to May during the period 1988-2013.
 306 Winter melt events mainly occur in the fall (October-November) and spring (April-May) months
 307 at high latitudes ($>60^{\circ}$ N) where continuous snow starts early and melts late in some years
 308 (Figure 5). During November to March for the period 1988-2013, no winter melt events are
 309 detected across large areas of Siberia and the Canadian and the Alaskan tundra where the
 310 monthly surface air temperature (SAT, from the Climatic Research Unit (University of East
 311 Anglia) CRUTem4 dataset [Jones et al., 2012]) is usually lower than -20° C (Figure 8). On
 312 average, April has the maximum extent and duration of winter melt events (Figure 7).

313

314 **3.3. Changes in snow cover and winter melt events**

315

316 The Mann-Kendall method is used for trend analysis taking into account serial correlation
 317 following Zhang et al. [2000]. Trends are only computed at grid cells with melt events detected
 318 in at least 12 winters. The PMW-derived estimates of changes in snow cover (MSOD, MMOD,
 319 and WPD) over the 1983-2013 period are shown in Figure 9. Most of the Arctic exhibits later
 320 snow onset trends, particularly over Scandinavia, western Russia, Alaska, Quebec and most



321 coastal areas (Figure 9a). The timing of the spring main melt onset date tends to be earlier over
 322 most of the Arctic except for northern Europe and western NA (Figure 9b). As a result, there are
 323 significant decreasing trends of more than 30 days in the duration of winter period over most of
 324 the Arctic (Figure 9c).

325

326 Over the study period, there are few significant trends in NMD over the Arctic (Figure 10a), and
 327 where there are significant trends, these tend to be dominated by decreases over northern Europe.
 328 The spatial distribution patterns of NMD trends contrast markedly between the PMW-varying
 329 and the PMW-fixed results (Figure 10a and b). Trends from PMW-fixed are dominated by
 330 increasing trends in NMD over most of the Arctic except for northern Europe. Trends from the
 331 reanalyses are not shown because the annual winter thaw frequency series from ERA-I and
 332 MERRA are not always consistent over the 1988-2013 period in some regions. For example over
 333 northern Quebec (not shown) the two series are well correlated over the period from 1980-2001
 334 ($r=0.75$) but diverge markedly after 2001 when numerous changes in data assimilation streams
 335 occurred in both reanalysis datasets [Rapaic et al. 2015]. This underscores the advantage of the
 336 PMW melt detection approach where a consistent time series of T_B are obtained from near
 337 identical sensors.

338

339 4. Discussion and conclusions

340

341 An algorithm for detecting winter melt events using satellite PMW measurements is developed
 342 and evaluated using in situ observations at weather stations and field surveys. The use of the high
 343 resolution (both spatially and temporally) surface-based radiometers and temperature profile data



344 highlight the fact that passive microwave radiometers are particularly sensitive to minute
345 amounts of liquid water present at the snow surface as is evident by the dramatic change in the
346 radiometric signal observed even when the recorded snow temperature (at 1 cm below the
347 surface) are still below 0° C. The winter T_BD algorithm has a higher success rate when the melt
348 duration last for multiple hours/days and/or the melt event has been preceded by warm air
349 temperatures. The algorithm does not reliably identify short duration melt events, ROS, or events
350 that occur immediately after or during extremely cold air/snowpack temperatures.

351

352 During the period 1988-2013, winter melt occurred at least once everywhere for north of 50°N.
353 On average, melt occurs less than one week per winter for most Arctic areas, with more melt
354 days (approximately two weeks per winter) occurring in areas with relatively long snow season
355 and temperate climate. Winter melt events are not detected in some areas of Siberia and the
356 Canadian and the Alaskan tundra where the monthly SAT is usually lower than -20°C. The
357 spatial distribution patterns of NMD are in general consistent from the reanalysis datasets (ERA-
358 I and MERRA) and PMW, while the detected NMDs are different probably due to biases in the
359 reanalysis datasets and the different methodology used to infer melt events.

360

361 Over the period 1988-2013, most of the Arctic exhibits later snow onset in fall, earlier melt onset
362 in spring, and thus decreasing duration of winter period. There are no significant trends in NMD
363 over most of the Arctic except for northern Europe where there are decreasing trends. The number
364 of melt days was observed to be significantly correlated with the duration of winter period over
365 most of the Arctic, particularly in regions where interannual variability in snow cover is higher
366 (Figure 11). Thus observed significant decreasing trends in WPD are playing a role in the



367 observed lack of significant increasing trends in NMD. A similar conclusion was reached by
 368 Cohen et al. [2015] in a study analyzing ROS event trends from reanalyses. They also found that
 369 the frequency of ROS events was correlated to large-scale modes of atmospheric circulation
 370 which contributes to regional-scale variability in ROS trends. Another contributing factor to the
 371 lack of increasing winter melt trends is the seasonal pattern of warming over Arctic land areas
 372 during 1988-2013, which is dominated by warming in the snow cover onset period (September -
 373 November) with comparatively little warming in the winter (December - February) and spring
 374 (March - May) period (Figure 12).

375

376 There is field evidence of changes in snowpack density and ice layers from a number of locations
 377 in the Arctic that is supported by an increased frequency of winter thaw events [Chen et al., 2013;
 378 Groisman et al., 2003; McBean et al., 2005; Johansson et al., 2011]. However, winter thaw
 379 events in some of these studies were inferred from air temperature observations [Groisman et al.,
 380 2003; McBean et al., 2005], which is different from results detected by PMW measurements.
 381 The lack of significant increasing trends in winter melt events observed in this study is also
 382 likely related to the relatively short period of data available for analysis and the dynamic
 383 mechanisms generating winter thaw and ROS events which tend to produce more random and
 384 chaotic environmental responses [Trenberth et al. 2015; Cohen et al. 2015]. This is underscored
 385 by trend analysis of annual numbers of winter thaws events in ERA-I and MERRA over a longer
 386 1980-2014 period (not shown) which revealed that locally significant increasing trends were only
 387 observed at 1% of snow covered land points in MERRA and 2% in ERA-I.

388



389 As previously pointed out in Figure 10b, the frequency of winter melt events is strongly
390 influenced by the method used to define WPD. A spatially and temporally varying definition of
391 WPD is required as the use of a fixed window generates artificial NMD trends from changes in
392 the timing of the snow cover season. This is further demonstrated in Figure 13 where monthly
393 NMD trends are computed using a fixed WPD of November-April. The results clearly
394 demonstrate that increases in NMD are being driven by trends during the snow cover shoulder
395 seasons of November-December and March-April and not the main winter period. A number of
396 studies reporting increasing NMD trends used fixed winter periods in their analysis [e.g.
397 Groisman et al., 2003; McBean et al., 2005].

398
399 The major advantage of the PMW winter melt event method presented here is that it is based on
400 physical processes in the snowpack (melt/freeze), unlike thaw events inferred from air
401 temperature observations that may or may not be associated with snowpack melt processes
402 depending on the thermal inertia of the snowpack. The PMW series is also consistent over time
403 unlike some reanalysis datasets. There is little evidence of significant trends in winter melt
404 frequency during the 1988-2013 period over most of the Arctic except for northern Europe
405 (decreasing trends).

406

407

408 **Acknowledgements.** The In-situ snow survey data used in this study was the result of multiple
409 campaigns over many years supported by numerous organizations which have provided direct
410 funding, logistical support or have contributed with people in the field. There have been too
411 many individual contributions to list them all here, so instead we will thank their affiliations



412 and/or their funding sources which include: Environment and Climate Change Canada, the
 413 Canadian Space Agency, University of Waterloo, Université de Sherbrooke, Wilfrid Laurier
 414 University, the Churchill Northern Study Centre, the Aurora Research Institute, the Canadian
 415 Foundation for Climate and Atmospheric Science, Manitoba Hydro, the Northwest Territories
 416 Power Corporation and Indian and Northern Affairs Canada. The following data centers are
 417 acknowledged for providing data: The National Snow and Ice Data Center for passive
 418 microwave satellite data, the National Climate Data Center for the Global Summary of the Day
 419 dataset, the Climatic Research Unit - University of East Anglia for the CRUtem4v gridded air
 420 temperature data, the European Centre for Medium-Range Weather Forecasts (ECMWF) for the
 421 ERA-interim data, and the Global Modeling and Assimilation Office (GMAO) at NASA
 422 Goddard Space Flight Center for MERRA data. The authors would like to thank Anne Walker
 423 for providing helpful comments to an early version of the manuscript.

424

425 **References**

426

427 Abdalati, W., Steffen, K., Otto, C., and Jezek, K. C.: Comparison of brightness temperatures
 428 from SSM/I instruments on the DMSP F8 and F11 satellites for Antarctica and the Greenland ice
 429 sheet, *Int. J. Remote Sens.*, 16, 1223–1229, doi:10.1080/01431169508954473, 1995.

430

431 AMAP: Snow, Water, Ice and Permafrost in the Arctic (SWIPA): Climate Change and the
 432 Cryosphere, Arctic Monitoring and Assessment Programme (AMAP), Oslo, Norway, xii +
 433 538pp, 2011.

434



- 435 Armstrong, R. L., Knowles, K. W., Brodzik, M. J., and Hardman, M. A.: DMSP SSM/I
436 Pathfinder Daily EASE-Grid Brightness Temperatures (1988–2013), Boulder, Colorado, USA,
437 National Snow and Ice Data Center, 1994.
438
- 439 Bartsch, A., Kumpula, T., Forbes, B. C., and Stammler, F.: Detection of snow surface thawing
440 and refreezing in the Eurasian Arctic with QuikSCAT: implications for reindeer herding, *Ecol.*
441 *Appl.*, 20, 2346–2358, 2010.
442
- 443 Bokhorst, S. F., Bjerke, J. W., Tømmervik, H., Callaghan, T. V, and Phoenix, G. K.: Winter
444 warming events damage sub - Arctic vegetation: Consistent evidence from an experimental
445 manipulation and a natural event, *J. Ecol.*, 97, 1408-1415, 2009.
446
- 447 Boon, S., Sharp, M., and Nienow, P.: Impact of an extreme melt event on the runoff and
448 hydrology of a high Arctic glacier, *Hydrol. Process.*, 17, doi: 10.1002/hyp.1194, 2003.
449
- 450 Brown, R. D. and Robinson, D. A.: Northern Hemisphere spring snow cover variability and
451 change over 1922–2010 including an assessment of uncertainty, *The Cryosphere*, 5, 219-229,
452 doi:10.5194/tc-5-219-2011, 2011.
453
- 454 Brown, R. and Lemay, M.: Climate variability and change in the Canadian Eastern Subarctic
455 IRIS region (Nunavik and Nunatsiavut), Chapter 2 in: Allard, M. and M. Lemay (Eds), Nunavik
456 and Nunatsiavut: From science to policy, An Integrated Regional Impact Study (IRIS) of climate
457 change and modernization, Arctic Net Inc., Quebec City, Canada, 303p, 2012.



458

459 Brown, R. D. and Derksen, C.: Is Eurasian October snow cover extent increasing? Environ. Res.

460 Lett., 8, 024006, doi:10.1088/1748-9326/8/2/024006, 2013.

461

462 Bulygina, O. N., Groisman, P. Y., Razuvaev, V. N., and Radionov, V. F.: Snow cover basal ice

463 layer changes over Northern Eurasia since 1966, Environ. Res. Lett., 5, 015004, doi:

464 10.1088/1748-9326/5/1/015004, 2010.

465

466 Callaghan, T.V., Johansson, M., Brown, R. D., Groisman, P. Y., Labba, N., Radionov, V., Barry,

467 R. G., Bulygina, O. N., Essery, R. L., Frolov, D. M., and Golubev, V. N.: The changing face of

468 Arctic snow cover: A synthesis of observed and projected changes, Ambio, 40, 17-31, 2011.

469

470 Chang, A., Foster, J., and Hall, D.: Nimbus-7 SMMR derived global snow cover parameters,

471 Ann. Glaciol., 9, 39– 44, 1987.

472

473 Cavalieri, D. J., Parkinson, C., DiGirolamo, N., Ivanoff, A.: Intersensor Calibration Between F13

474 SSMI and F17 SSMIS for Global Sea Ice Data Records, NASA technical report, 13pp, 2012.

475

476 Chen, W., Russell, D. E., Gunn, A., Croft, B., Chen, W. R., Fernandes, R., Zhao H., et al.:

477 Monitoring habitat condition changes during winter and pre-calving migration for Bathurst

478 Caribou in northern Canada, Biodivers., 14, 36-44, 2013.

479



480 Cohen, J., Ye, H. and Jones, J.: Trends and variability in rain-on-snow events, *Geophys. Res.*
 481 *Lett.*, 42, 7115-7122, 2015.

482

483 Dee, D. P., Uppala, S. M., Simmons, A. J., Berrisford, P., Poli, P., Kobayashi, S., ... Vitart, F.:
 484 The ERA-Interim reanalysis: Configuration and performance of the data assimilation system, *Q.*
 485 *J. R. Meteorol. Soc.*, 137, 553–597, doi:10.1002/qj.828, 2011.

486

487 Derksen, C., Sturm, M., Liston, G., Holmgren, J., Huntington, H., Silis, A., et al.:
 488 Northwest Territories and Nunavut snow characteristics from a sub-Arctic traverse:
 489 Implications for passive microwave remote sensing, *J. Hydrometeorol.*, 10, 448–463, 2009.

490

491 Derksen, C., Toose, P., Lemmetyinen, J., Pulliainen, J., Langlois, A., Rutter, N., Fuller, M. C.:
 492 Evaluation of passive microwave brightness temperature simulations and snow water equivalent
 493 retrievals through a winter season, *Remote Sens. Environ.*, 117, 236-248, 2012.

494

495 Derksen, C., Lemmetyinen, J., Toose, P., Silis, A., Pulliainen, J., Sturm, M.: Physical properties
 496 of Arctic versus subarctic snow: Implications for high latitude passive microwave snow water
 497 equivalent retrievals, *J. Geophys. Res.*, 119, 7254–7270, doi:10.1002/2013JD021264, 2014.

498

499 Grenfell, T. C. and Putkonen, J.: A method for the detection of the severe rain-on-snow event on
 500 Banks Island, October 2003, using passive microwave remote sensing, *Water Resour. Res.*, 44
 501 W03425, 2008.

502



503 Groisman, P. Y., Sun, B., Vose, R. S., Lawrimore, J. H., Whitfield, P. H., Førland, E., Hanssen-
 504 Bauer, I., Serreze, M. C., Razuvaev, V. N. and Alekseev, G. V.: Contemporary climate changes
 505 in high latitudes of the Northern Hemisphere: daily time resolution, Proc. 14th AMS Symp. on
 506 Global Change and Climate, 1-10, 2003.

507

508 Hansen, B. B., Aanes, R., Herfindal, I., Kohler, J. and Saether, B. E.: Climate, icing, and wild
 509 arctic reindeer: past relationships and future prospects, Ecology, 92, 1917–23, 2011.

510

511 Hay, L. E. and McCabe, G. J.: Hydrologic effects of climate change in the Yukon River Basin,
 512 Clim. Chang., 100, 509-523, 2010.

513

514 Johansson, C., Pohjola, V. A., Jonasson, C., and Callaghan, T.V.: Multi-decadal changes in snow
 515 characteristics in sub-Arctic Sweden, Ambio, 40, 566-74, 2011.

516

517 Jones, P. D., Lister, D. H., Osborn, T. J., Harpham, C., Salmon, M. and Morice, C. P.:
 518 Hemispheric and large-scale land surface air temperature variations: an extensive revision and an
 519 update to 2010, J. Geophys. Res., 117, D05127, doi:10.1029/2011JD017139, 2012.

520

521 Kim, Y., Kimball, J. S., McDonald, K. C., and Glassy, J.: Developing a global data record
 522 of daily landscape freeze/thaw status using satellite passive microwave remote sensing, IEEE
 523 Trans. Geosci. Remote Sens., 49, 949–960, doi:10.1109/TGRS.2010.2070515, 2011.

524



- 525 Liston, G. E. and Elder, K.: A meteorological distribution system for high resolution terrestrial
 526 modeling (MicroMet), J. Hydrometeorol., 7, 214-234, 2006.
- 527
- 528 Liston, G. E. and Hiemstra, C. A.: The Changing Cryosphere: Pan-Arctic Snow Trends (1979–
 529 2009), J. Climate, 24, 5691–5712, doi: <http://dx.doi.org/10.1175/JCLI-D-11-00081.1>, 2011.
- 530
- 531 Markus, T., Stroeve, J. C., and Miller, J.: Recent changes in Arctic sea ice melt onset, freeze-up,
 532 and melt season length, J. Geophys. Res., 114, C12024, doi:10.1029/2009JC005436, 2009.
- 533
- 534 McBean, G., Alexeev, G., Chen, D., Førland, E., Fyfe, J., Groisman, P. Y., King, R., Melling, H.,
 535 Vose, R., and Whitfield, P. H.: Arctic climate: past and present, Arctic Climate Impact
 536 Assessment, Cambridge, Cambridge University Press, chapter 2, 21–60, 2005.
- 537
- 538 Nghiem, S. V., Hall, D. K., Foster, J. L., and Neumann, G.: Terrestrial Snow, In: Njoku E. (Ed.)
 539 Encyclopedia of Remote Sensing, Springer-Verlag Berlin Heidelberg, 0, doi:
 540 10.1007/SpringerReference_327235, 2014.
- 541
- 542 Pedersen, S. H., Liston, G. E., Tamstorf, M. P., Westergaard-Nielsen, A., and Schmidt, N. M.:
 543 Quantifying Episodic Snowmelt Events in Arctic Ecosystems, Ecosystems, 1-18, 2015.
- 544
- 545 Rapaic, M., Brown, R., Markovic, M., and Chaumont, D.: An evaluation of temperature and
 546 precipitation surface-based and reanalysis datasets for the Canadian Arctic, 1950-2010, Atmos.-
 547 Ocean, 53, 283-303, doi:10.1080/07055900.2015.1045825, 2015



548

549 Rees, A., Lemmetyinen, J., Derksen, C., Pulliainen, J. and English, M.: Observed and modeled
 550 effects of ice lens formation on passive microwave brightness temperatures over snow covered
 551 tundra, *Remote Sens. Environ.*, 114, 116–26, 2010.

552

553 Rennert, K. J., Roe, G., Putkonen, J., and Bitz, C. M.: Soil thermal and ecological impacts of rain
 554 on snow events in the circumpolar Arctic, *J. Climate*, 22, 2302–15, 2009.

555

556 Rienecker, M. M., and Coauthors : MERRA: NASA's Modern-Era Retrospective Analysis for
 557 Research and Applications, *J. Climate*, 24, 3624–3648, doi:10.1175/JCLI-D-11-00015.1, 2011.

558

559 Semmens, K. A., Ramage, J., Bartsch, A., and Liston, G. E.: Early snowmelt events: detection,
 560 distribution, and significance in a major sub-arctic watershed, *Environ. Res. Lett.*, 8, doi:
 561 10.1088/1748-9326/8/1/014020, 2013.

562

563 Serreze, M. C., Barrett, A. P., and Stroeve, J.: Recent changes in tropospheric water vapor over
 564 the Arctic as assessed from radiosondes and atmospheric reanalyses, *J. Geophys. Res.*, 117,
 565 D10104, doi:10.1029/2011JD017421, 2012.

566

567 Stroeve, J., Maslanik, J., and Li, X.: An intercomparison of DMSP F11- and F13-derived sea ice
 568 products, *Remote Sens. Environ.*, 64, 132–152, doi:10.1016/S0034-4257(97)00174-0, 1998.

569

570 Tedesco, M.: Snowmelt detection over the Greenland ice sheet from SSM/I brightness



571 temperature daily variations, *Geophys. Res. Lett.*, 34, L02504, doi: 10.1029/2006GL028466,
 572 2007.

573

574 Trenberth, K. E., Fasullo, J. T., Shepherd, T. G.: Attribution of climate extreme events, *Nat.*
 575 *Clim. Chang.*, 5, 725-730, doi: 10.1038/nclimate2657, 2015.

576

577 Wang, L., Wolken, G., Sharp, M., Howell, S., Derksen, C., Brown, R., Markus, T., and Cole, J.:
 578 Integrated pan-Arctic melt onset detection from satellite active/passive microwave measurements,
 579 2000–2009, *J. Geophys. Res.*, 116, doi:10.1029/2011JD016256, 2011.

580

581 Wang, L., Derksen, C., and Brown, R., and Markus, T.: Recent changes in pan-Arctic melt onset
 582 from satellite passive microwave measurements, *Geophys. Res. Lett.*, 40, 522–528,
 583 doi:10.1002/grl.50098, 2013.

584

585 Wilson, R. R., Bartsch, A., Joly, K., Reynolds, J. H., Orlando, A., and Loya, W. M.: Frequency,
 586 timing, extent, and size of winter thaw-refreeze events in Alaska 2001–2008 detected by
 587 remotely sensed microwave backscatter data, *Polar Biol.*, doi:10.1007/s00300-012-1272-6, 2012.

588

589 Ulaby, F., Moore, R., and Fung, A.: *Microwave Remote Sensing: Active and Passive*, Vol. 2,
 590 Norwood, Massachusetts, Artech House, 1986.

591

592 Zhang, X., Vincent, L. A., Hogg, W. D., and Niitsoo, A.: Temperature and precipitation trends in
 593 Canada during the 20th century, *Atmos.–Ocean*, 38, 395–429, doi:10.1080/



594 07055900.2000.9649654, 2000.



Table 1. Data periods for the different satellite passive microwave radiometers and overpass used for melt detection in this study.

Satellite	Start Date	End Date	Overpass
F-08 SSM/I	Jul 1988	Dec 1991	Descending
F-11 SSM/I	Jan 1992	May 1995	Ascending
F-13 SSM/I	May 1995	Dec 2008	Ascending
F-17 SSMIS	Jan 2009	present	Ascending



Table 2. Performance summary of the satellite melt detection using the winter T_B D algorithm at snowpit survey sites across Canada, characterized with coincident nearby weather station air temperatures.

Survey Site		Snowpit Feature Depths (cm)			Satellite Melt Detection		Weather Station Air Temperature (°C)					
Weather Station / Year of Survey	Lat/Lon	Pit Depth	Melt Feature Height Above Ground	DOY	DOY	Reason for Success/Failure	DOY	Melt Event # of HRS	Avg. Temp	Previous 36 HR Avg. Temp	Min. Temp	Prior Day Max. Temp
Thompson, MB 2005	56.016N 97.260W	53	Melt-freeze crust	9-8	070	321 Warm snow	321	27	0.37	1.35	-4.5	6.8
				45-43		034 Warm snow	033	8	1.44	-2.69	-5.5	-1.8
Gillam, MB 2005	57.020N 94.140W	63	Melt-freeze crust	53-52.5	070	034 Warm snow	033	9	0.49	-5.75	-10.5	-2.7
Rae Lakes, NT 2006	63.882N 115.072W	72	Ice layer	36	094	Not Detected Cold snow	082	10	3.7	-7.3	-17.9	6.5
			Melt-freeze crust	62			092	1	1.1	-11.03	-28.3	-1.9
			Sun crust	72								
Daring Lake, NT 2007	64.867N 111.573W	48	Ice layer	48-47.5	100	Not Detected Rain event / Cold snow	098	2	0.3	-6.47	-13.62	-6.4
Fort McPherson, NT 2008	67.569N 133.618W	No Lower Layer Melt Features Present			097	Not Detected Cold snow	020	26*	3.7*	-25.0*	-27.1*	-23.6*
		54	Ice layer	41			093	32*	2.9*	-3.57*	-13.0*	6.1*
				49								
			Melt-freeze crust	54-53.5			095	4*	2.88*	-0.83*	-7.5*	4.7*
LaGrande IV, QC 2009	53.648N 73.875W	72	Melt-freeze crust	39.5-39	078	Not Detected Cold snow	362	5	-0.3	-11.20	-27.7	-6.3
			Ice layer	70-69.5		Not Detected Rain event / Cold Snow	076	17	2.45	-19.60	-33.4	-10.6
Churchill, MB 2010	58.7364N 93.8227W	69	Ice layers - multiple	54-45	102	090 Warm snow	090	6**	0.5**	-2.83**	-5.1**	-1.92**
			Melt-freeze/rain crust	69-66		099 Warm snow	099	13**	5.4**	-1.32**	-9.31**	8.76**

* Indicates that the weather station data is available only during daylight hours (recorded by observer), thus average values are not comparable to other stations

** Indicates that air temperatures from a local meteorological station were used instead of the Churchill Climate Station (local met station was closer to the snowpit)

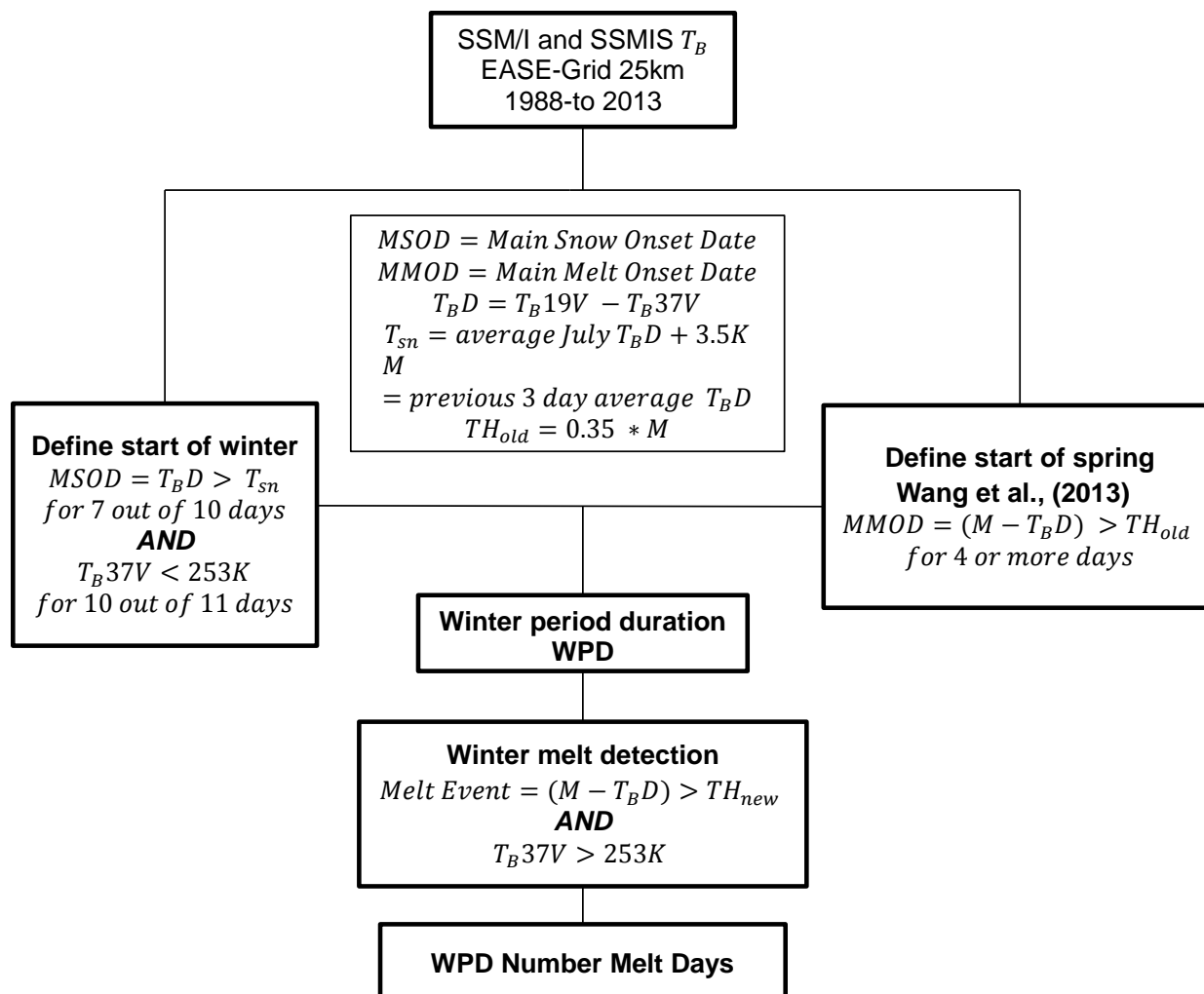


Figure 1. Schematic flow chart of the winter $T_B D$ melt detection method for PMW satellite data.

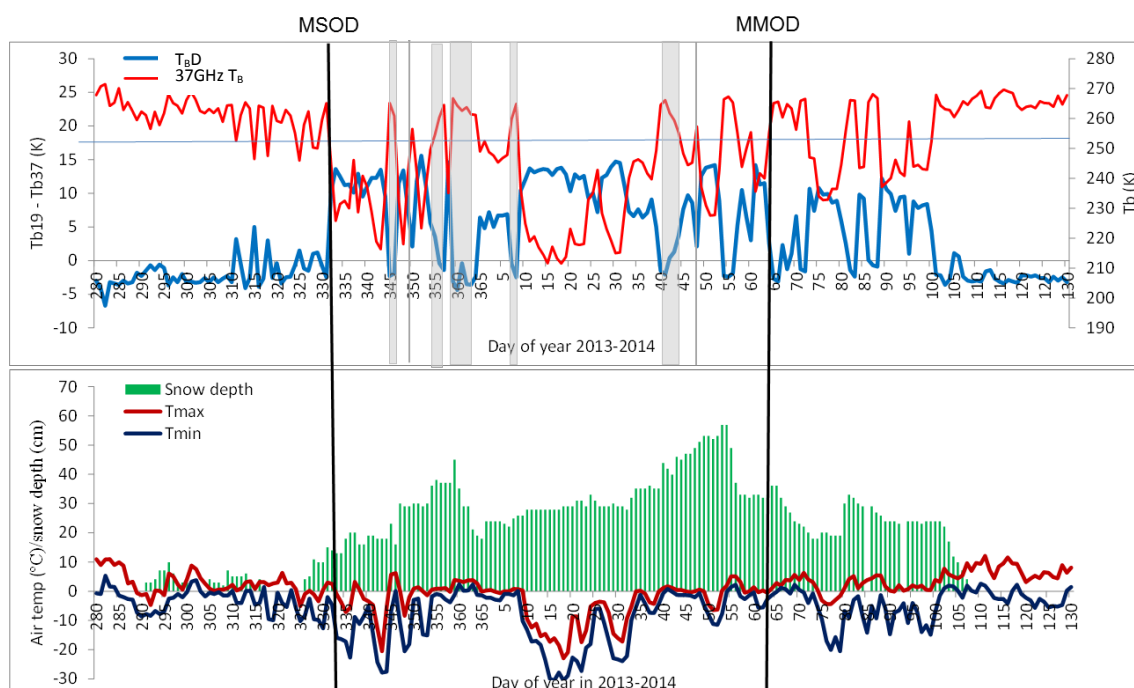


Figure 2. Example of time series of SSM/I $T_{B,D}$ (a) and daily surface air temperature (°C) /snow depth (cm) (b) at Pudasjarvi, Finland (65.4°N, 26.97°E) during the 2013- 2014 winter. The vertical grey lines/bars in (a) represent melt events detected by satellite.

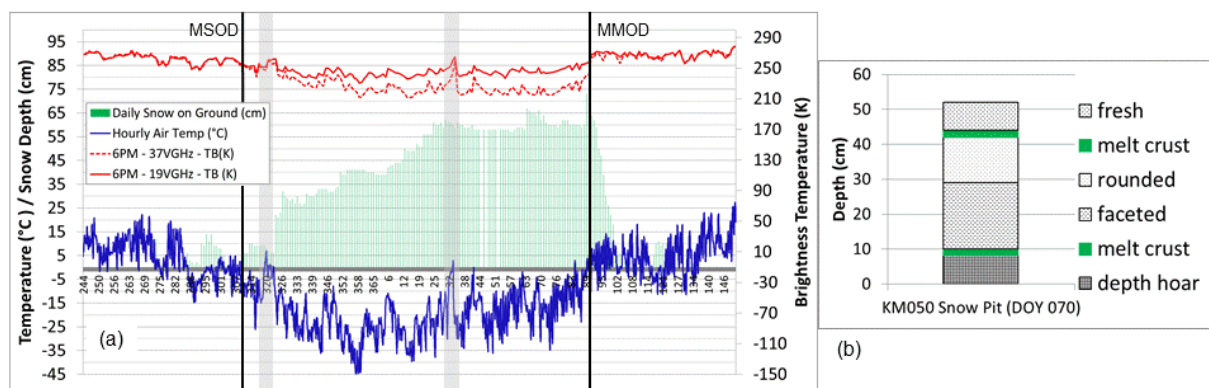


Figure 3. (a) Time series of hourly air temperature and daily snow depth and T_B at the Thompson, Manitoba Meteorological Station from Sep. 2004 to May 2005; the shaded grey bars highlight the timing of the melt events detected by the PMW satellite data. (b) Snow stratigraphy from the KM050 snow pit site surveyed on DOY097. Note that both the early season and recent melt crusts observed in the snowpit agree reasonably well with the timing of two winter melt events recorded at the Thompson airport and detected by the PMW satellite data.

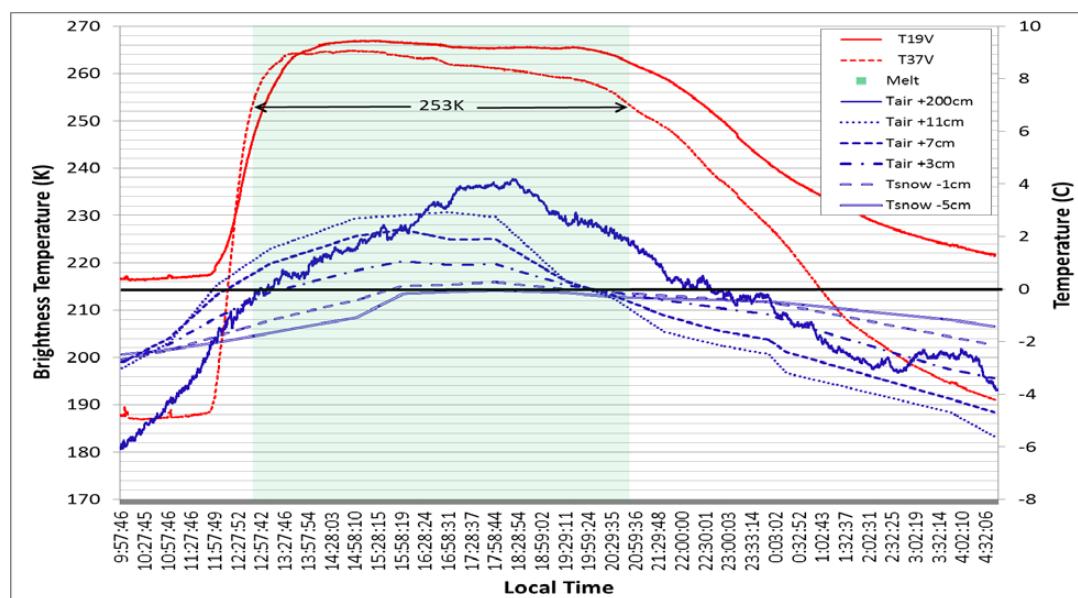


Figure 4. Time series of the surface-based radiometer T_B and the air/snow temperature measurements recorded during the April 12-13, 2010 diurnal melt event. The green shaded region highlights the period when the winter T_B D algorithm successfully detected a winter melt event, the onset of which coincides very closely with the 2 m air temperature sensor.

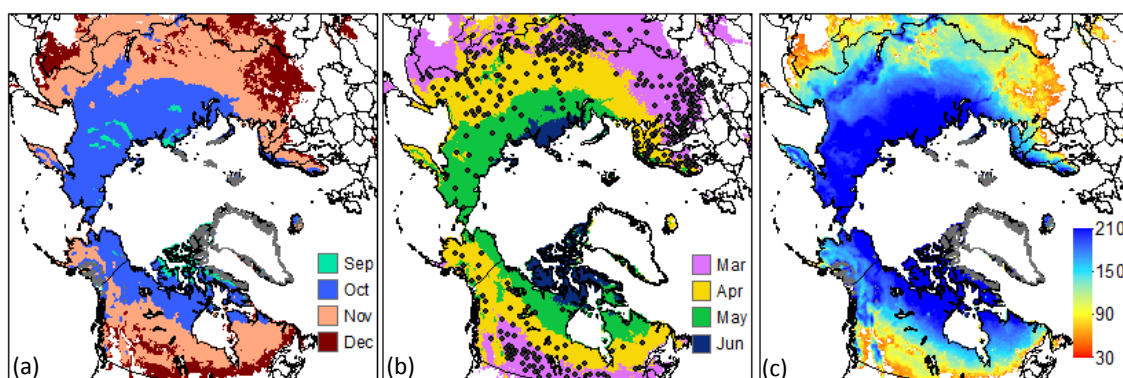


Figure 5. The mean main snow onset date in fall (a), main melt onset date in spring (b), and mean winter period duration (days) (c) during the period 1988-2013. The black dots in (b) represent WMO weather stations used for algorithm development and evaluation.

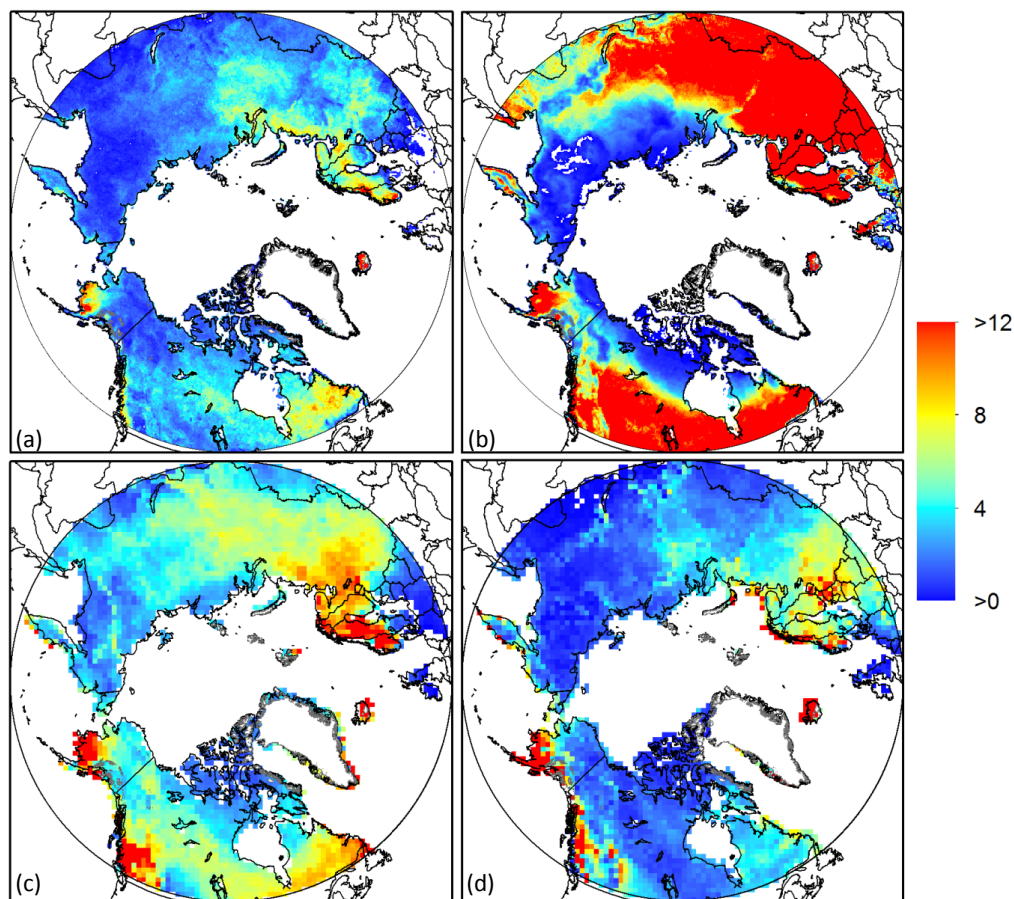


Figure 6. The average annual number of melt days over 1988-2013 from (a) PMW using a varying winter period; (b) PMW using a fixed winter period (November to April); (c) ERA-Interim; and (d) MERRA.

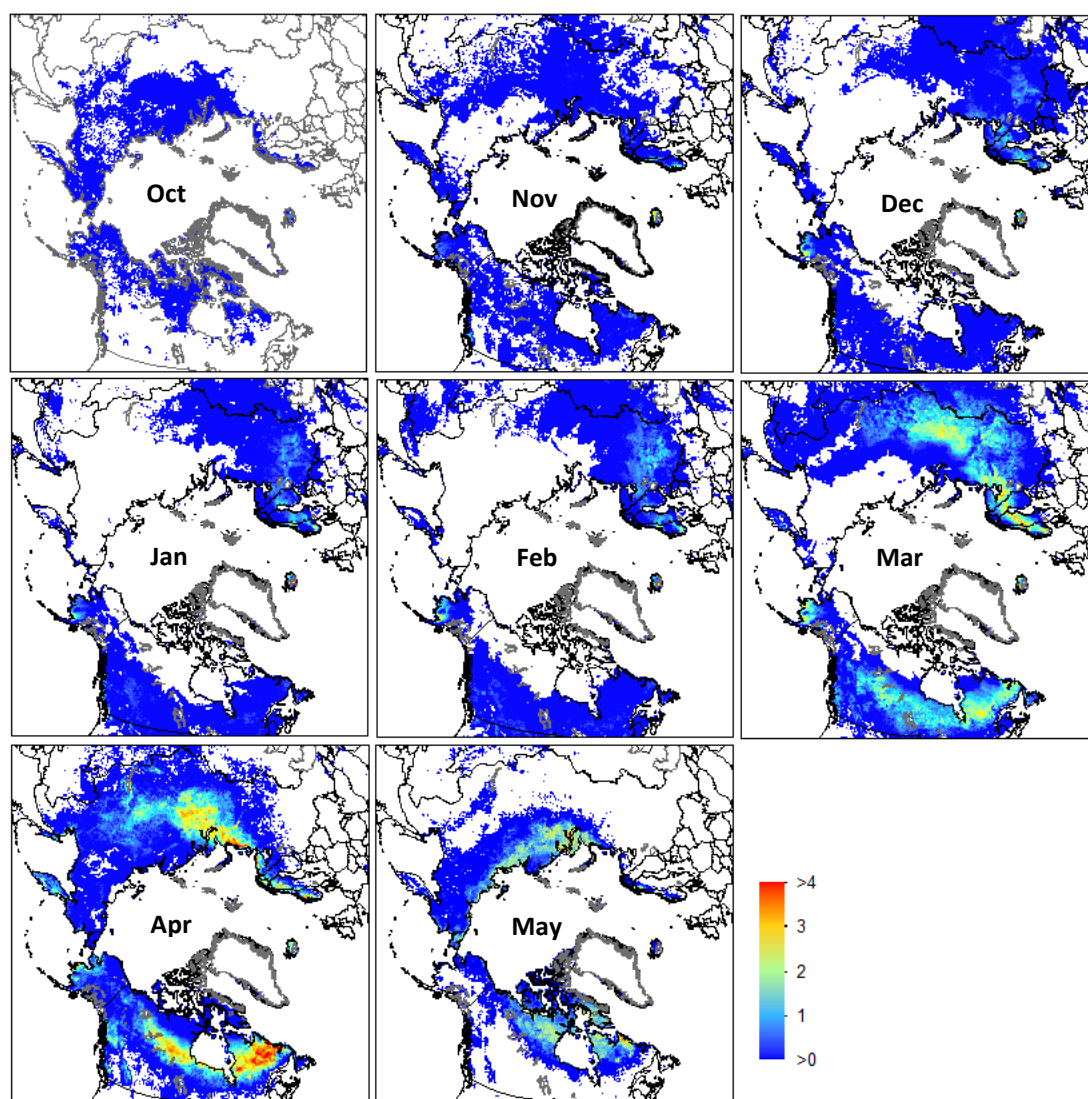


Figure 7. Monthly mean number of melting days from PMW during the period 1988-2013.

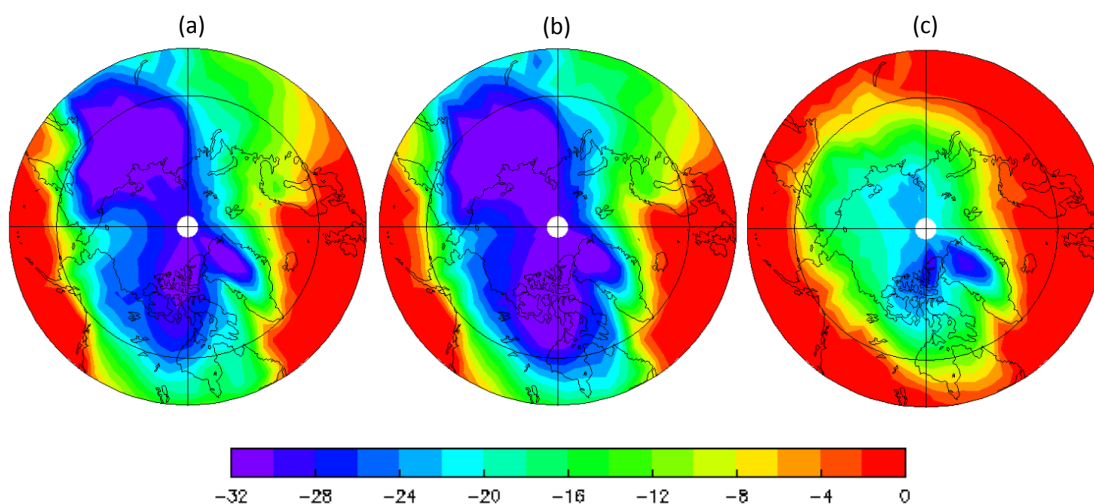


Figure 8. The climatological mean surface air temperature from CRUTem4 during the period 1961-1990 for (a) December, (b) February, and (c) April.

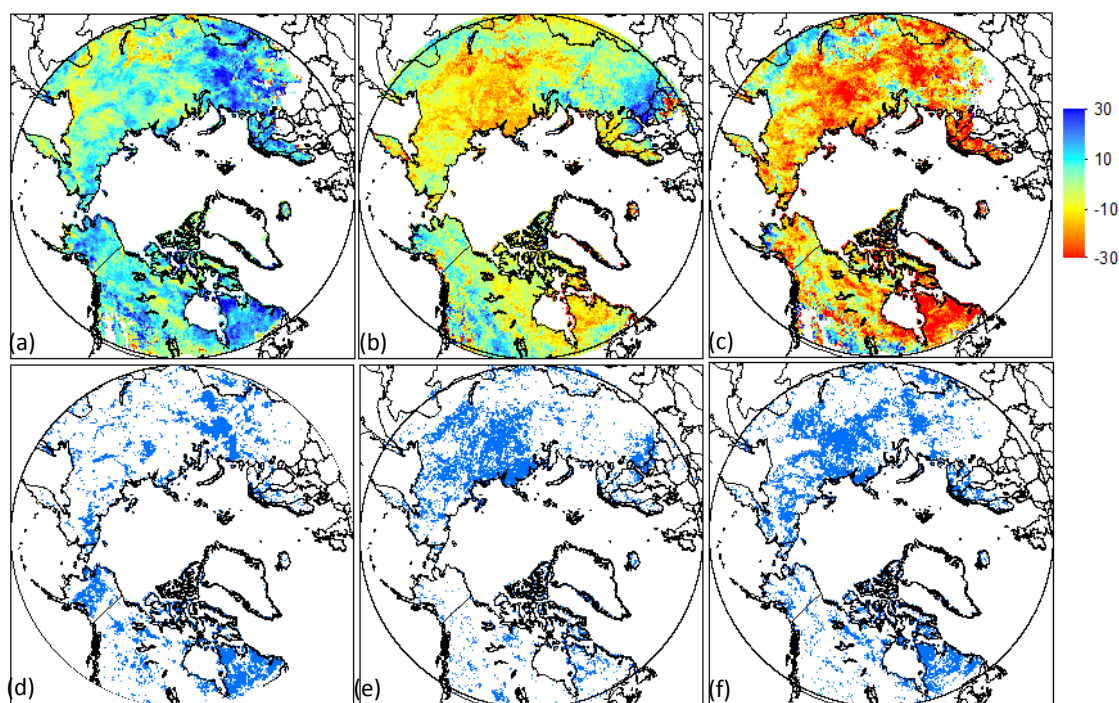


Figure 9. Mann-Kendall trends (days/26yr) over the period 1988-2013 in (a) MSOD, (b) MMOD, (c) WPD. Grid cells with trends statistically significant at the 90% level are shown in (d) MSOD, (e) MMOD, and (f) WPD.

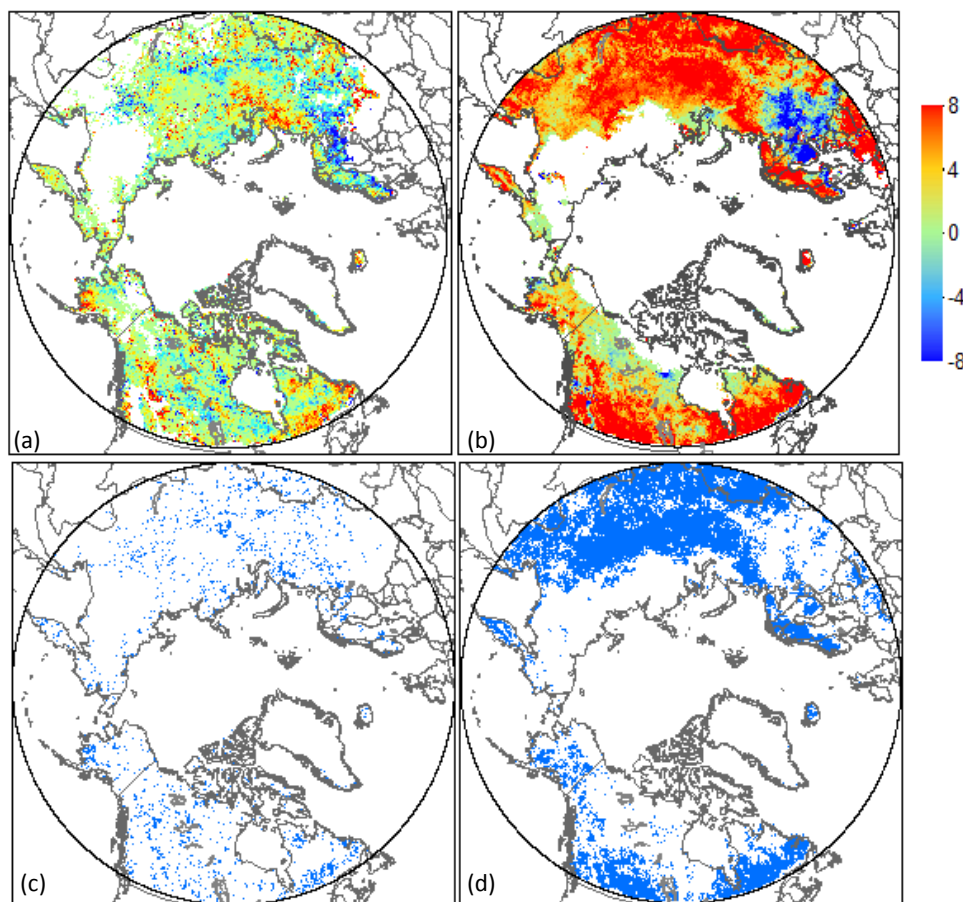


Figure 10. Mann-Kendall trends (days/26yr) over the period 1988-2013 in the number of winter melt days from (a) PMW; (b) PMW-fixed; (c) and (d) show grid cells with trends statistically significant at the 90% level in (a) and (b) respectively.

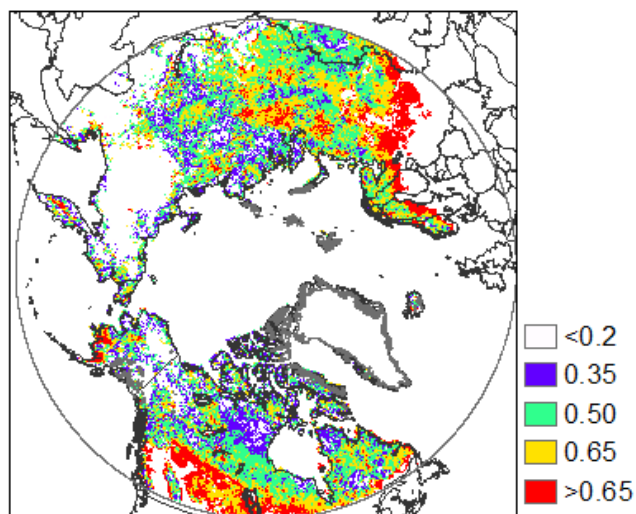


Figure 11. The correlation coefficient between number of melt days and the duration of winter period from PMW during 1988-2013.

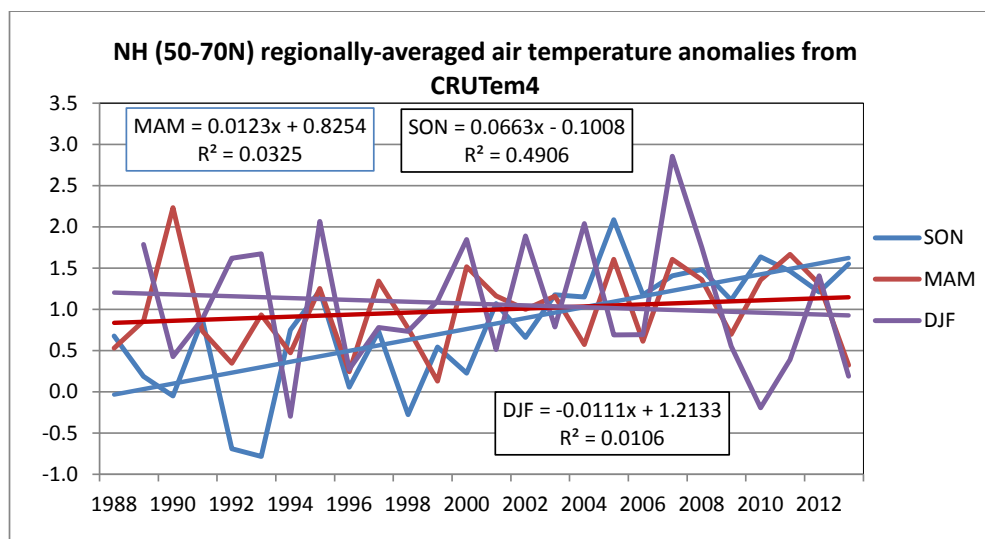


Figure 12. Time series of surface air temperature and trends in Northern Hemisphere land areas during the period 1988-2013. Note that the September-October-November (SON) period warmed more than the March-April-May (MAM) and December-January-February (DJF) periods.

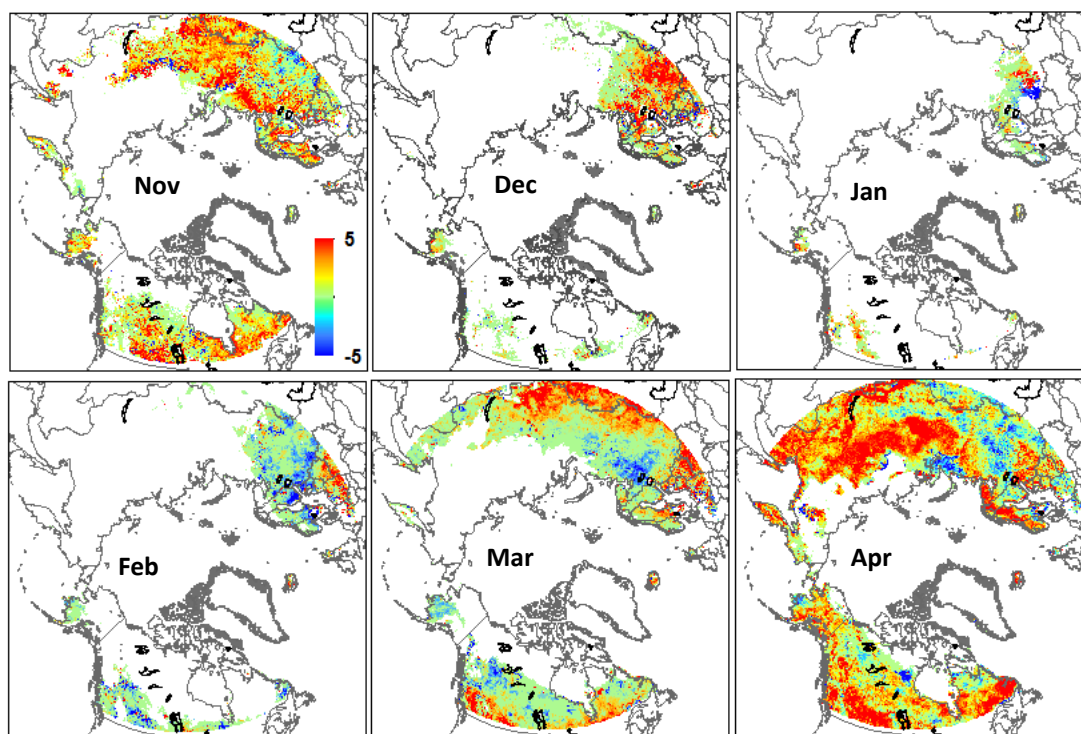


Figure 13. Mann-Kendall trends (days/26yr) in the number of melt days derived by PMW-fixed from November to April during the period 1988-2013.